Rock and Soil Mechanics

Volume 42 | Issue 7 Article 6

11-23-2021

# Response analysis of residual soil slope considering crack development under drying–wetting cycles

Yue LIU
*Fujian Key Laboratory of Geohazard Prevention, Fuzhou, Fujian 350002, China*

Dong-xia CHEN
*Xiamen Engineering Technology Center for Intelligent Maintenance of Infrastructure, Xiamen, Fujian 361005, China*

Hui WANG
*Administrative Committee of Dujiangyan Economic Development Zone, Dujiangyan, Sichuan 611830, China*

Jia-jing YU
*Department of Civil Engineering, Xiamen University, Xiamen, Fujian 361005, China*

Rock and Soil Mechanics 2021 42(7): 1933−1943 ISSN 1000−7598
https: //doi.org/10.16285/j.rsm.2020.6504 rocksoilmech.researchcommons.org/journal

# Response analysis of residual soil slope considering crack development under drying−wetting cycles

LIU Yue[1, 2], CHEN Dong-xia[1, 3], WANG Hui[4], YU Jia-jing[1]

1. Department of Civil Engineering, Xiamen University, Xiamen, Fujian 361005, China
2. Fujian Key Laboratory of Geohazard Prevention, Fuzhou, Fujian 350002, China
3. Xiamen Engineering Technology Center for Intelligent Maintenance of Infrastructure, Xiamen, Fujian 361005, China
4. Administrative Committee of Dujiangyan Economic Development Zone, Dujiangyan, Sichuan 611830, China

**Abstract:** In order to study the response of granite residual soil slope with cracks under different number of drying-wetting cycles (D−W cycles), model test was carried out and the crack width expansion index was quantified by investigating the crack images. Based on the direct shear test, the calculation formulas of soil strength degradation and crack depth were developed. Then, the model test and the numerical simulation results were compared to analyze the response of the residual soil slope considering crack extension. The results showed that the fractures width expansion in residual soil under D−W cycles followed the Logistic model, and there was a quantitative relationship between fracture depth and strength degradation. The fracture depth tended to be stable with the increase of D−W cycles. When the number of D−W cycles was small, the change of moisture content at the bottom of the slope lags significantly behind that at the top and the middle of the slope, however, the change of moisture content at each position of the slope tended to be the same with the increase of D−W cycles. The deformation at the bottom and the middle of the slope with the crack expansion tended to be the same compared to the slope without cracks, however, the deformation at the top area was larger, which led to the increase of the deformation gap between the top and bottom of the cracked slope.

**Keywords:** drying-wetting cycles; granite residual soil; crack; water content; deformation

## 1 Introduction

Granite residual soil is widely distributed in the southeast coast of China. These areas have abundant rainfall and frequent alternation of drying and wetting[1], which leads to the continuous drying-wetting cycles (D−W cycles) of residual soil, causes serious loss of internal cementitious materials and a significant decrease of cohesion[2−3]. Under the D−W cycle, the structure of soil will suffer from fatigue damage such as clay reduction, pore coarsening and loose structure, which is easy to produce cracks in the drying process, showing the characteristics of brittle failure and damage[4−6]. The existence of fissures will destroy the integrity of soil structure, weaken the strength of soil and increase its permeability[6−11]. In slope engineering, fissures not only increase the risk of rainwater infiltration, reduce its safety factor[12], but also increase the evaporation rate of water and aggravate soil erosion[13]. Under the condition of extreme precipitation, the development of fissures is accelerated and the slope is unstable[14].

The crack evolution behavior can be characterized by the parameters such as the node, number, and area of cracks[15]. Computer image processing technology is an important way to study the crack propagation[16−18]. Earlier in the qualitative analysis of the crack propagation, Lu et al. [19] used CT technology to obtain the relationship between the crack evolution and volume deformation of remolded expansive soil under the action of D−W cycle. Meanwhile, they obtained that the crack expands with the increase of times of the D−W cycle. Zhang et al. [20] found that the degree of cracks development is greatly affected by the permeability and size of soil through the D−W test of expansive soil. Combined with MIP method, Cheng et al. [21] elaborated the crack development during the drying process from the microscopic perspective, and found that the crack development of soil samples with complete structure has a linear relationship with the decrease of water content, and the local propagation of main cracks and secondary cracks of soil samples with scattered structure is more obvious, and the geometric parameters of cracks show two-stage linear propagation characteristics. In quantitative

Received: 10 October 2020 Revised: 9 April 2021
This work was supported by the Opening Fund of Key Laboratory of Geohazard Prevention of Hilly Mountains, Ministry of Natural Resources (Fujian Key Laboratory of Geohazard Prevention) (FJKLGH2021K004) and the Opening Fund of Xiamen Transportation Infrastructure Intelligent Management Engineering Technology Research Center= (TCIMI201804).
First author: LIU Yue, male, born in 1996, Master candidate, mainly engaged in research on residual soil foundation pit or slope stability. E-mail: 25320181152857@stu.xmu.edu.cn

analysis, Tang et al. [22] developed crack image analysis system (CIAS), which automatically quantifies parameters including the area of cracks, length, width, number of cracks, angle, fractal dimension, number of intersections, surface fracture rate and probability density function, providing a powerful tool for the crack research. Hu et al. [23] defined a disturbance function which was consistent with the logistic function to predict the local development and distribution of cracks in the sample. Wang et al. [24] obtained the evolution law of soil cracks under natural evaporation by IPP image processing technology, and established the Boltzmann growth curve model of cracks development length and water content. Meanwhile, the development of cracks is accompanied by the structural damage of soil, resulting in the decrease of soil strength under D−W cycles. Wei et al. [25] discussed the influence of cracks development on soil shear strength in the quantitative analysis of cracks network under D−W cycles. Chen[26] studied the crack evolution law of red clay under the action of D−W cycles, and obtained that the relationship between shear strength index and fracture density of red clay under the action of D−W cycle is quadratic polynomial. Tang et al.[27] analyzed expansive soil with different water content, quantitatively characterized the relationship between the crack morphology and unconfined compressive strength of soil, and pointed out that there was a competitive relationship between the contribution of suction to strength and the decrease of cracks to strength.

The theoretical analysis of cracks propagation is mainly considered the fact that the tensile stress of soil at crack tips is greater than the tensile strength of soil. Lu et al.[28] found that the tensile strength of unsaturated soil is significantly affected by the cohesion of soil. It is easy to cause the decrease of the cohesion of soil, the decrease of the tensile strength of soil and the acceleration of cracks propagation. Shi et al.[29-30] quantified the relationship between the crack propagation and D−W cycles, and derived the calculation formula of the crack depths with D−W cycles and water content as the main parameters. Then, the calculation formula of the crack depths is deduced from the perspective of damage, which theoretically improves the crack propagation law of expansive soil under the action of D−W cycle. Thi et al.[31] took the crack as viscoelastic damage unit and numerically simulated the crack propagation of cohesive soil during the drying process, which further verified the close relationship between the crack propagation and physical mechanical properties of soil.

Previous studies mainly focused on expansive soil. Granite residual soil is different from expansive soil in mineral loss and easy disintegration due to its special formation conditions and particle composition. In the existing slope stability analysis, the influence of the crack development under D−W cycles is seldom considered. Therefore, the purpose of this paper is to study the evolution law and mechanism of cracks in granite residual soil under D−W cycles. On this basis, the response of slope with cracks is discussed by using model test and finite element numerical calculation method. This research aims to provide new ideas and methods for the analysis and treatment of slope with cracks.

## 2 Model test of slope under D−W cycles

The granite residual soil slope model is built in the laboratory, different D−W cycle conditions are simulated, and the crack propagation on the top of the slope is recorded by image shooting. Meanwhile, the strength parameters of the soil in the slope after each D−W cycle are measured, and the crack propagation law of the slope under different D−W cycles is obtained.

### 2.1 Slope model preparation

The granite residual soil near a student apartment in Xiamen city is used in the test, and the model test is conducted on the slope with 30° masonry toe. The physical parameters of the soil used in the test are shown in Table 1.

**Table 1 The physical parameters of soil**

| Saturated water content /% | Maximum dry density /(g • cm$^{-3}$) | Plastic limit /% | Liquid limit /% | Plasticity index | Relative density |
|---|---|---|---|---|---|
| 24.2 | 1.78 | 20 | 47 | 27 | 2.72 |

The model box is composed of two identical compartments, which are filled in layers to form a slope, as shown in Fig. 1. the large and small D−W cycles are set in the left and right compartments considering that the rainfall in Xiamen region is concentrated in spring and summer, respectively[32]. Meanwhile, the changes of water content are 12.5%−24.0% and 17.5%−24.0% in the left and right compartments, respectively, and five D−W cycles are conducted. Four moisture sensors are installed on the left and right slopes, respectively, corresponding to the top (KM1, KM5), middle (KM2, KM3, KM6, KM7) and bottom (KM4, KM8) of the slope. The installation depth of the moisture sensor is 8 cm. The specific installation location is shown in Fig. 2.

https://rocksoilmech.researchcommons.org/journal/vol42/iss7/6
DOI: 10.16285/j.rsm.2020.6504

(a) Front view (b) Side view

**Fig. 1 Photos of slope model**

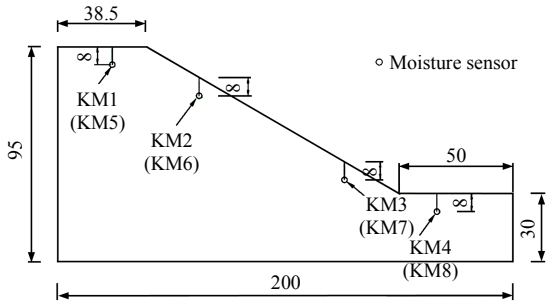


(a) Side view

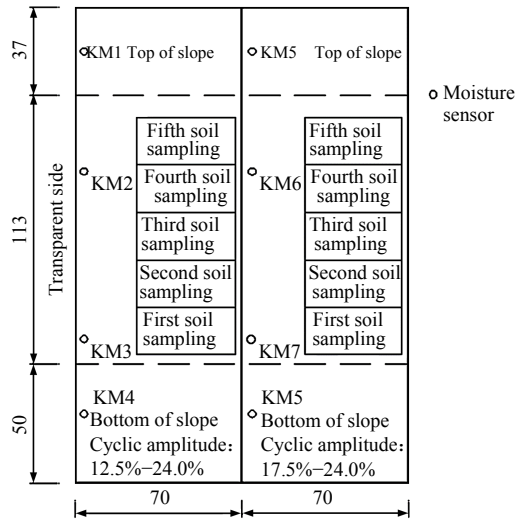


(b) Top view

**Fig. 2 Sketches of the slope model (unit: cm)**

### 2.2 Drying-wetting system

During the humidification process, tap water is pumped by water pump and humidified by sprinkler. A total of 8 sprinkler heads are set, 4 on the left and 4 on the right, as shown in Fig. 3 (a). When all nozzles are turned on, the amount of water spraying is 2.7 L/min, the corresponding rainfall intensity is 16 mm/h, and the rainfall duration is 2 h, that is, the rainfall of 32 mm in 24 h, which is equivalent to heavy rain. In the process of humidification, intermittent water addition is used to avoid the formation of runoff on the surface of the slope due to the slow infiltration of the slope and the erosion of the slope, resulting in the failure of the slope model. In the model test, 6 high-power bulbs and 4 basket heaters were used for drying. Hanging the dryer directly above the slope with a string and adjusting its height to maintain the surface temperature of the slope at about 40 ℃ to simulate the effect of sunlight, as shown in Fig. 3 (b).

The test process was controlled by controlling the water content at the depth of 8 cm below the slope surface under each D−W cycle. The change of water content with times of D−W cycles is shown in Fig. 4 (the actual abscissa in Fig. 4 is time/d, and the time after each drying cycle is taken as the counting point of cycle number).

(a) Humidifier (b) Drying device

**Fig. 3 Drying and wetting equipment**

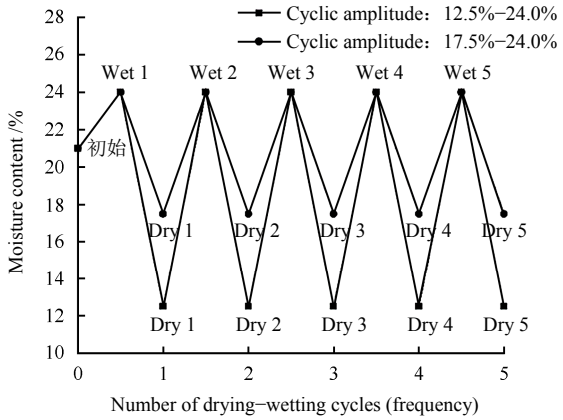


**Fig. 4 Change of water content during drying and wetting cycles**

## 3 The crack development under D−W cycles

### 3.1 The effect of D−W cycle on the crack width

At the end of each drying cycle, a camera set up at a fixed position on the top of the slope is used to take photos of the top of the slope, and the development of cracks under different D−W cycles is recorded, as shown in Fig. 5.

In this paper, the ratio of the area of cracks to the area of the slope top is used to define the fracture degree:

$$\delta_{\mathrm{f}} = \frac{\sum_{i=1}^{n} A_i}{A} \times 100\% \quad (1)$$

where $\delta_f$ is the fracture degree; $A$ is the area of soil in the photo; and $A_i$ is the area of the $i^{th}$ crack.

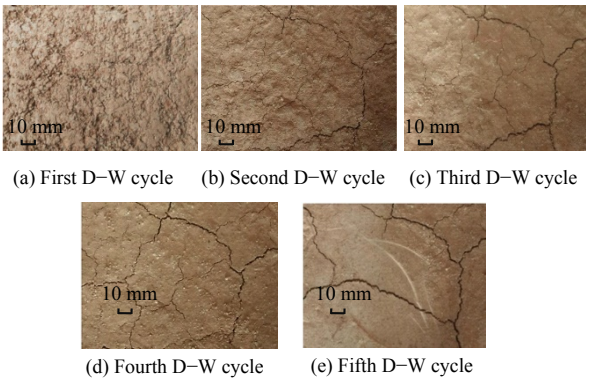


(a) First D−W cycle (b) Second D−W cycle (c) Third D−W cycle

(d) Fourth D−W cycle (e) Fifth D−W cycle

**Fig. 5 Crack propagation at the top of slope under large amplitude drying-wetting cycles (12.5%−24.0%)**

After each D−W cycle, the crack image is binarized and decluttered by MATLAB, and the proportion of black pixels in the whole image area is counted as the fracture degree. Taking the crack development after the fifth large cycle as an example, the treatment process is shown in Fig. 6. The treatment results of all working conditions are shown in Table 2.


(a) Surface crack image after stabilization (b) Surface crack image after binarization

**Fig. 6 Binarization and vectorization of crack images (after the large fifth D−W cycles)**

**Table 2 Parameters of cracks on the top of slope under D−W cycles**

| D−W cycles amplitude | cycles /time | Black pixel number | The total pixels number | Fracture degree $\delta_f$/% |
|---|---|---|---|---|
| | 1 | 689 | | 0.64 |
| | 2 | 1 250 | | 1.16 |
| 17.5%−24% | 3 | 2 156 | 107 804 | 2.00 |
| | 4 | 2 996 | | 2.78 |
| | 5 | 3 891 | | 3.61 |
| | 1 | 453 | | 0.44 |
| | 2 | 1 380 | | 1.34 |
| 12.5%−24% | 3 | 3 008 | 103 044 | 2.92 |
| | 4 | 3 555 | | 3.45 |
| | 5 | 3 781 | | 3.67 |

After obtaining the fracture degree, the growth curve is used to express the relationship between the crack propagation and times of D−W cycles[24]. Logistic model was used in this test, and the fitting formula was as follows:

$$y = A_2 + \frac{A_2 - A_1}{1 + \left(\frac{x}{x_0}\right)^{p'}} \tag{2}$$

where $A_1$ and $A_2$ are the model fitting parameters; $p'$ is the parameter related to soil properties (dry density, porosity, saturation, et al.); $x_0$ is a parameter related to the water content of soil after D−W cycles; $x$ is an independent variable related to times of D−W cycles; $y$ is the strain that related to the fracture degree. The relationship between the fracture degree and times of D−W cycles is shown in the following formula after fitting the test data, and the fitting results are shown in Fig. 7.

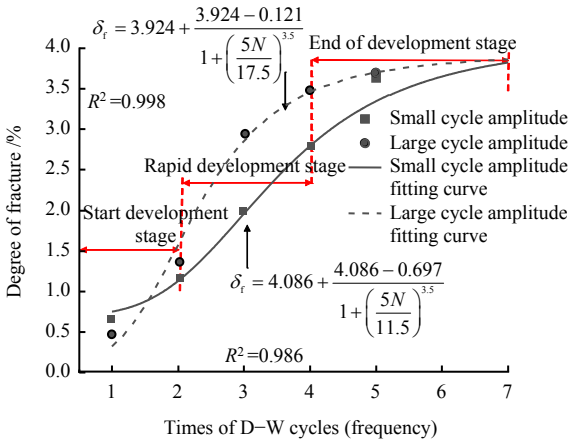


**Fig. 7 Fitting relation between the fracture degree and times of D−W cycles**

$$\delta_f = A_2 + \frac{A_2 - A_1}{1 + \left(\frac{5N}{w_d}\right)^{3.5}} \tag{3}$$

where $N$ is times of D−W cycles; $w_d$ is the water content on dry side. In small cycle amplitude, $A_1$= 0.697 and $A_2$=4.086; in large circulation amplitude, $A_1$=0.121 and $A_2$=3.924. And the "d" in the $w_d$ resprents the meaning of drying.

It can be seen from Fig. 7 that the crack propagation goes through three stages, from the initiation stage to the propagation stage, and finally to the equilibrium stage. This is similar to the results presented in the literatures [4, 24]. Meanwhile, the fracture degree corresponding to large cyclic amplitude expands more rapidly, but the fracture degree under the two cyclic amplitude tends to be the same. The main reasons are as follows:

Figure. 8 (a) is a schematic diagram of the initial state of residual soil. The grain size of granite residual soil is mainly focused on more than 0.5 mm and less than 0.074 mm, and the total amount of coarse and

fine particles is close, while the content of medium particles is less. The grain size distribution determines the fabric of granite residual soil. The framework of residual soil is composed of coarse particles, which are wrapped and filled by clay particles. Due to the small content of medium fine sand and silt filled in the coarse-grained skeletons, the macrospores are larger, the initial cracks are wider, and the intra granular cracks are also developed. The crack propagation of residual soil is mainly due to the cyclic expansion and contraction of clay minerals and the reciprocating migration of micro pore water in the process of D−W cycle, which changes the expansion potential and matrix potential, and then leads to the fatigue damage of soil microstructure (pore coarsening, cement hydrolysis, crack breeding, et al.). Figure. 8 (b) shows the humidification process of residual soil. When water invades, clay particles dissolve into water, and the hydrolysis of cementitious materials will weaken the original cohesion and solidified cohesion. Meanwhile, water migration is accompanied by the loss of fine particles and the expansion of clay particles, resulting in the widening of initial cracks in the soil. The drying process is shown in Fig. 8 (c). Due to water evaporation and transportation, the particles in the soil contract unevenly, resulting in the tensile stress. When it accumulates to the tensile strength thresholds of soil, the weak part of the soil is pulled off, driving the meso-crack propagation[4−5]. Moreover, the larger the D−W cycle amplitude, the more severe the damage of soil microstructure is, which is indicated by the faster crack propagation.

After a certain number of D−W cycles (after the fifth cycle in this test), the final soil humidification state is shown in Fig. 8(d). With the loss of clay minerals and the dissipation of its hydrophilic capacity, the swelling potential will basically remain unchanged after the continuous attenuation, while the cohesion and tensile capacity of the corresponding soil remain stable after the decrease. The loss of clay and fine particles in the soil is serious, forming a through water transport channel, which provides conditions for the development of the main cracks in the subsequent drying process. Figure. 8(e) shows the final state of soil drying. The reduction of clay particles leads to the weakening of tensile stress. As long as the breakthrough area is formed, the main cracks can be started with less reserve of tensile stress. A small number of secondary cracks are cut off by the existing main cracks and can not expand after propagation, and then the propagation of soil cracks reaches the equilibrium stage. Therefore, the crack propagation of residual soil tends to be consistent under different D−W cycles.

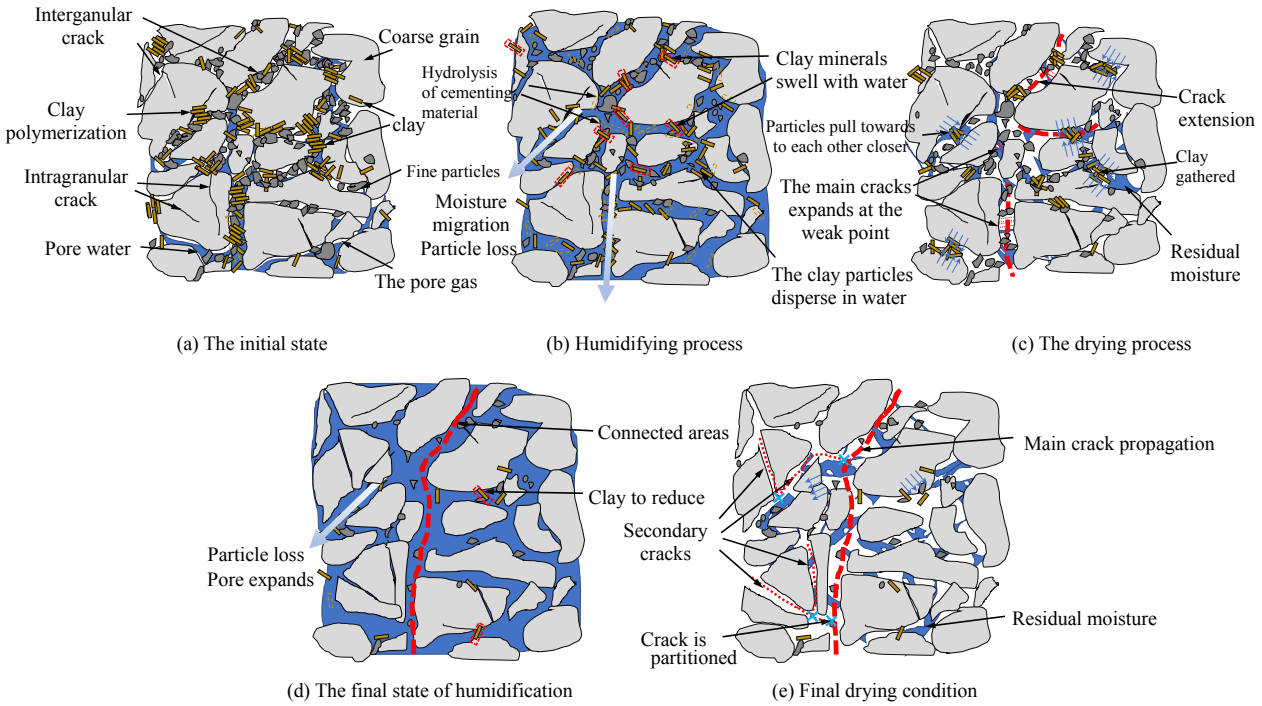


**Fig. 8 Schematic diagram of residual soil structure evolution under D−W cycles**

### 3.2 Influence of D−W cycles on soil strength

After the humidification process completed, five ring cutter samples are cut from the slope model. The location and sequence of soil samples are shown in Fig. 2. The slow shear test was conducted using quadruple direct shear apparatus, and the shear strength at the depth of 8 cm under the slope under different vertical loads (50, 100, 200, 300, 400 kPa) was measured. The

cohesion and the internal friction angle of soil samples were obtained, which are listed in Table 3.

**Table 3 Shear strength parameters under D−W cycles**

| Case number | Cohesion $c$ /kPa | Friction angel $\varphi$/(°) | Case number | Cohesion $c$ /kPa | Friction $\varphi$/(°) |
|---|---|---|---|---|---|
| SDW-1 | 73.5 | 28.9 | BDW-1 | 70.2 | 27.8 |
| SDW-2 | 60.4 | 27.9 | BDW-2 | 58.6 | 27.8 |
| SDW-3 | 57.6 | 27.9 | BDW-3 | 52.1 | 26.2 |
| SDW-4 | 54.8 | 26.4 | BDW-4 | 48.8 | 26.2 |
| SDW-5 | 52.7 | 24.7 | BDW-5 | 46.7 | 26.7 |

Note: SDW(BDW)-$N$ indicates the $N^{\text{th}}$ D−W cycle of small cycle (large cycle).

The experimental data were fitted by using the initial cohesion ($c_0$), cycle amplitude ($\Delta w$) and times of D−W cycles ($N$). The relationship between the cohesion and times of D−W cycle was obtained. The relationship between the amplitude of D−W cycle is as follows:

$$c = c_0\left[1 - p\cdot\Delta w\ln(qN+1)\right] \quad (4)$$

where $p$ and $q$ are fitting parameters. In this test, the parameters in the large cyclic amplitude test are as follows: $\Delta w$=11.5%, $p$=0.16, $q$=1.88, $R^2$=0.996; the parameters in the small cyclic amplitude test are as follows: $\Delta w$=6.5%, $p$=0.09, $q$=5.44, $R^2$=0.994. When the initial number of cycles is 0, $c$ is equal to $c_0$. The corresponding fitting curve is plotted in Fig. 9.

It can be seen from Fig. 9 that the correlation coefficients of the two fitting curves are greater than 0.99, indicating that the fitting formula can accurately describe the variation law of soil cohesion with times of D−W cycles. Meanwhile, the decrease of cohesion under different cycle amplitude is the largest after the first D−W cycle, and then gradually slows down. The results show that the decrease of soil cohesion under the influence of large cyclic amplitude is greater than that under the influence of small cyclic amplitude, and the change ranges are 33.5% and 28.3% respectively, which indicates that the greater the D−W cyclic amplitude is, the greater the decrease of soil strength is.

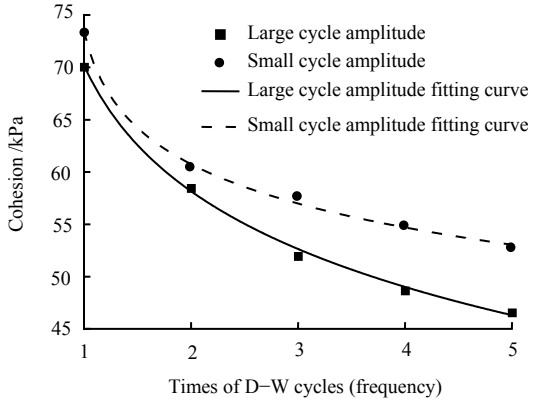


**Fig. 9 Relationship between cohesion and number of D−W cycles**

### 3.3 Calculation of crack propagation depth under D−W cycles

When the horizontal stress in the soil is greater than the tensile strength of the soil, the cracks propagation. Some scholars believe that the negative half axis of the Mohr-Coulomb strength curve is the tensile strength of soil (that is, $\sigma_{\text{tia}}$ in Fig. 10). However, Lu et al. [28] believed that the ratio of normal stress to shear stress was consistent with that under compression (that is, $\tan\varphi$), soil failure was a manifestation of shear failure when the ratio of normal stress to shear stress reached the limit, as shown in point a in Fig. 10.

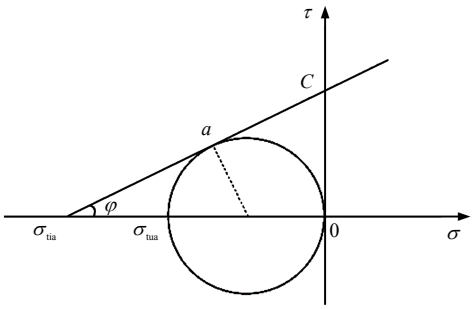


**Fig. 10 Mohr-Coulomb strength curve**

Therefore, the normal stress of the Mohr circle corresponding to point a when the shear stress is 0 is regarded as the uniaxial tensile strength of soil:

$$\frac{c}{\sigma_{\text{tia}}} = \tan\varphi \quad (5)$$

$$\frac{c}{\sigma_{\text{tua}}} = \frac{1}{2\tan\left(\frac{\pi}{4}-\frac{\varphi}{2}\right)} \quad (6)$$

where $\sigma_{\text{tua}}$ is the theoretical uniaxial tensile strength.

Lu et al. [28] compared the tensile strength and uniaxial tensile strength of sand, and the ratio of actual tensile strength and uniaxial tensile strength of sand is 0.48. However, Tang et al [33]'s experimental study on the tensile strength of granite residual soil shows that the ratio of actual tensile strength to uniaxial tensile strength is 0.43, that is:

$$\frac{\sigma_{\text{tut}}}{\sigma_{\text{tua}}} = 0.43 \quad (7)$$

where $\sigma_{\text{tut}}$ is the actual uniaxial of soil.

Substituting Eqs. (4)−(6) into Eq. (7), the following equation is obtained.

$$\sigma_{\text{tut}} = 0.86c_0\left[1 - p\cdot\Delta w\ln(qN-q+1)\right]\tan\left(\frac{\pi}{4}-\frac{\varphi}{2}\right) \quad (8)$$

According to Hooke's law, the stress-strain relationship in soil is as follows:

$$\varepsilon_{\mathrm{v}}=\frac{\sigma_{\mathrm{v}}-u_{\mathrm{a}}}{E}-\frac{2\mu}{E}\left(\sigma_{\mathrm{h}}-u_{\mathrm{a}}\right)-\frac{1-2\mu\chi\left(u_{\mathrm{a}}-u_{\mathrm{w}}\right)}{E} \quad (9)$$

$$\varepsilon_{\mathrm{h}}=\frac{\sigma_{\mathrm{h}}-u_{\mathrm{a}}}{E}-\frac{\mu}{E}\left(\sigma_{\mathrm{v}}+\sigma_{\mathrm{h}}-2u_{\mathrm{a}}\right)-\frac{1-2\mu\chi\left(u_{\mathrm{a}}-u_{\mathrm{w}}\right)}{E} \quad (10)$$

where $\sigma_{\mathrm{v}}$ is the stress in the vertical direction; $u_{\mathrm{a}}$ is pore air pressure; $u_{\mathrm{w}}$ is pore water pressure; $\sigma_{\mathrm{h}}$ is the stress in the horizontal direction; $\mu$ is Poisson's ratio; $\chi$ is the effective stress parameter; $E$ is the elastic modulus of soil. Among them, the "v" in the $\sigma_{\mathrm{v}}$ resprents the meaning of vertical, the "h" in the $\sigma_{\mathrm{h}}$ resprents the meaning of horizontal, the "a" in the $u_{\mathrm{a}}$ resprents the air, and the "w" in the $u_{\mathrm{w}}$ resprents the water.

Assuming that the soil is in the state of failure, according to Eqs. (9) and (10), the horizontal stress can be expressed as the following equation.

$$\sigma_{\mathrm{h}}-u_{\mathrm{a}}=\frac{\mu}{1-\mu}\left(\sigma_{\mathrm{v}}-u_{\mathrm{a}}\right)-\frac{1-2\mu}{1-\mu}\chi\left(u_{\mathrm{a}}-u_{\mathrm{w}}\right) \quad (11)$$

When the horizontal stress reaches the tensile strength, the soil will be damaged and the crack will expand until the horizontal stress of the soil at the crack tip is equal to the tensile strength of the soil, reaching the limit equilibrium state, that is,

$$\sigma_{\mathrm{h}}-u_{\mathrm{a}}=\sigma_{\mathrm{tut}} \quad (12)$$

Substituting Eqs. (8) and (11) into Eq. (12) leads to the following equation:

$$\begin{aligned}&\frac{\mu}{1-\mu}\left(\sigma_{\mathrm{v}}-u_{\mathrm{a}}\right)-\frac{1-2\mu}{1-\mu}\chi\left(u_{\mathrm{a}}-u_{\mathrm{w}}\right)=\\&-0.86c_0\left[1-p\cdot\Delta w\ln(qN-q+1)\right]\tan\left(\frac{\pi}{4}-\frac{\varphi}{2}\right)\end{aligned} \quad (13)$$

where minus indicates tension.

Assuming that $u_{\mathrm{a}}=0$, then $\sigma_{\mathrm{v}}-u_{\mathrm{a}}=\gamma z$, where $\gamma$ is the unit weight of soil. The matric suction decreases linearly from the ground surface down. The matric suction at the groundwater level $H$ decreases to 0, and the matric suction at the arbitrary depth $z$ can be expressed as:

$$u_{\mathrm{a}}-u_{\mathrm{w}}=S_0\left(1-\frac{2}{H}\right) \quad (14)$$

Substituting Eq. (13) into Eq. (14) leads to the maximum crack propagation depth ($z_{\mathrm{c}}$)

$$z_{\mathrm{c}}=\frac{-0.86c\tan\left(\frac{\pi}{4}-\frac{\varphi}{2}\right)+\frac{1-2\mu}{\mu}\chi S_0}{\frac{\mu}{1-\mu}\gamma+\frac{(1-2\mu)\chi S_0}{\mu H}} \quad (15)$$

where $c$ can be calculated by Eq. (4).

## 4 Numerical simulation of slope with cracks under D−W cycles

Geo-studio software was used to build the numerical models for the above model test. The effect of D−W cycles on the stability of granite residual soil slope considering with and without cracks was discussed.

### 4.1 Calculation model and boundary conditions

The physical parameters of soil measured in model tests (see Table 1) were used to establish the calculation model. The Mohr-Coulomb model was adopted as the constitutive model of slope soil, and the soil-water characteristic curve model of residual clay in Xiamen area was adopted, as shown in Fig. 11.

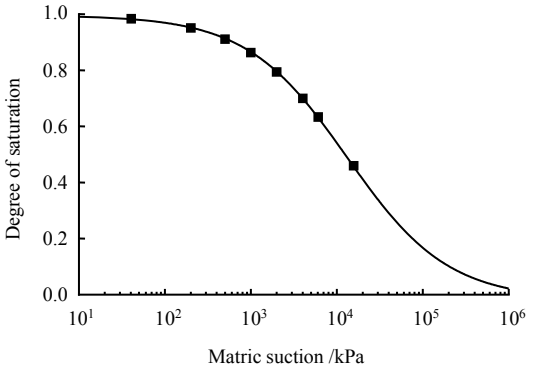


**Fig. 11 Soil-water characteristic curve of unsaturated residual soil in Xiamen**

The geometric size is set in the same proportion as the size of the actual model. The underground water level is at 0 m, and the right boundary of the slope bottom is set as the permeable boundary to limit the displacement on both sides of the slope. Meanwhile, 16 mm/h unit discharge was set on the surface of the top, middle and bottom of the slope to simulate precipitation, and the precipitation time was 2 h. The site climate interaction was set at 40 ℃ to simulate the drying process. When the water content at the depth of 0.8 m of the model slope reached the designed water content, the drying was stopped.

### 4.2 Processing of the crack areas

Tensile cracks are easily generated on the slope crest during the collapse of granite residual soil and the preparation process of landslide[33]. In the calculation of this paper, only fully developed cracks are considered at the top of the slope, and no fully developed main cracks exist at the middle and bottom of the slope. For the crack propagation depth corresponding to the numerical simulation condition, the calculation formula of the maximum crack propagation depth derived above and the calculation formula in reference [35] are adopted respectively, and the comparison of the obtained results

is shown in Fig. 12. It can be seen from the Fig. 12 that the calculation results of the crack depth in this paper are close to those in the references, indicating the rationality of the calculation formula of the crack growth depth (Eq. (15)).

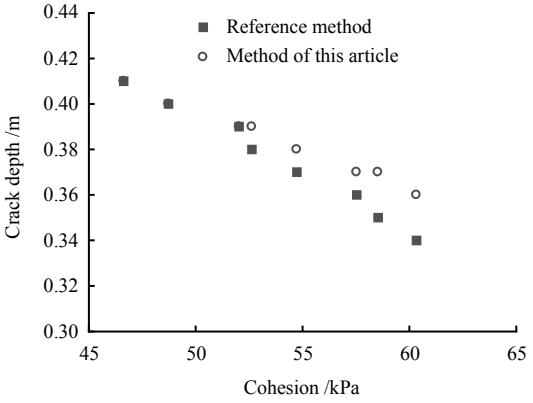


**Fig. 12 Relationship between the crack depth and the cohesion**

After the tensile crack depth at the top of the slope is obtained by the above method, the range of the main crack (as shown in Fig. 13) is determined. The material in the main crack area has no cohesion and the internal friction angle is 0. Each layer of soil mechanics parameters are determined according to the following steps: considering the influence depth of each D−W cycle, the slope soil is divided into three layers[36]. The first layer is the fully influenced layer, its strength is fully attenuated, its thickness is 2/3 of the maximum propagation depth of cracks after each cycle, and its cohesion is the soil cohesion $c_i$ after each cycle ($i$ represents the time of D−W cycles). The second layer is the transition layer, the crack is not fully developed, the thickness of the crack is 1/3 of the maximum expansion depth, the cohesion is $c_b = (c_i + c_0)/2$, these two layers together constitute the fracture zone. The third layer is the undisturbed soil layer, the thickness from the bottom of the transition layer to the bottom of the slope, cohesion is $c_0$. Because the D−W cycle has little effect on the internal friction angle of the soil, the internal friction angle of the three layers is 27°. The slope model considering the effect of cracks is shown in Fig. 13.

Under the influence of D−W cycles, the permeability of soil will increase[37]. Based on the variation of saturated permeability coefficient and the soil-water characteristic curve of residual soil in Table 4 after each D−W cycle, the function of the permeability coefficient of soil after D−W cycle was calculated as shown in Fig.14.

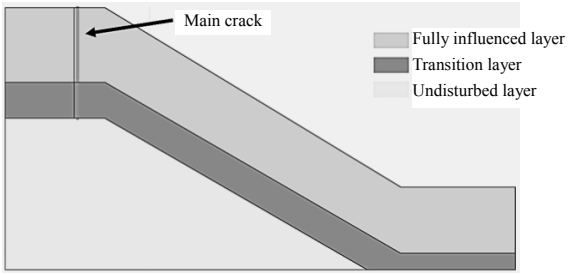


**Fig. 13 Numerical simulation model**

**Table 4 Parameters of crack area**

| Case number | Saturated permeability coefficient /(m • s$^{-1}$) | Case number | Saturated permeability coefficient /(m • s$^{-1}$) |
|---|---|---|---|
| SDW-1 | $5.0\times10^{-7}$ | BDW-1 | $5.0\times10^{-7}$ |
| SDW-2 | $9.0\times10^{-7}$ | BDW-2 | $9.0\times10^{-7}$ |
| SDW-3 | $1.2\times10^{-6}$ | BDW-3 | $1.2\times10^{-6}$ |
| SDW-4 | $1.4\times10^{-6}$ | BDW-4 | $1.4\times10^{-6}$ |
| SDW-5 | $1.5\times10^{-5}$ | BDW-5 | $1.5\times10^{-5}$ |

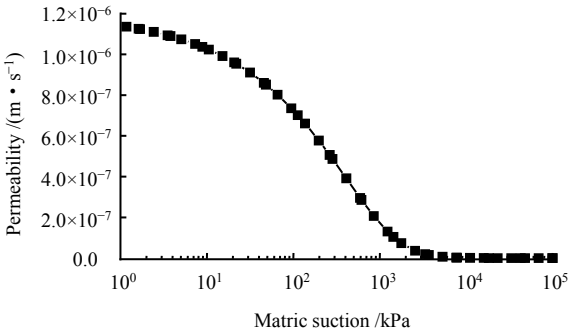


**Fig. 14 Permeability coefficient function of BDW-3**

Meanwhile, the crack causes anisotropy of soil permeability, that is, the permeability coefficient increases by 3-4 orders of magnitude along the crack direction[38]. Crack induced anisotropy is reflected by the angle between the crack plane and the vertical direction $\alpha$. In reference [39], the parameter $\alpha$ = 26.5° in the simulation software is set to simulate the crack permeability direction under the most unfavorable state.

## 5 Response analysis of slope with cracks under D−W cycles

### 5.1 Response of water content

The change data of water content at the top, middle and bottom of the slope in the numerical model were collected, and the change of water content of the water sensor at each position in the model test was compared. The results are shown in Figs. 15 and 16.

According to Fig. 15, with the increase of D−W cycles, the change of water content on the slope surface increases. Numerical model was conducted to simulate crack propagation at the top of the slope, where the

water content changes the most. In the first drying cycle, the water content at the top of the slope decreased to 17.9% after drying for 9 h, compared with that at the middle and bottom of the slope without the main cracks. The change rate of water content on the slope and the bottom of the slope is slow, but it is similar to the change of water content in the model test. With the increase of times of D−W cycles, the variation of water content at the top of the slope is more consistent with the variation trend of the model test, because cracks develop gradually during the model test. As the time of D−W cycle increases, cracks begin to appear on the surface of the slope, which gradually widen and deepen and extend into the interior of the slope, increasing water evaporation channels and accelerating evaporation rate.

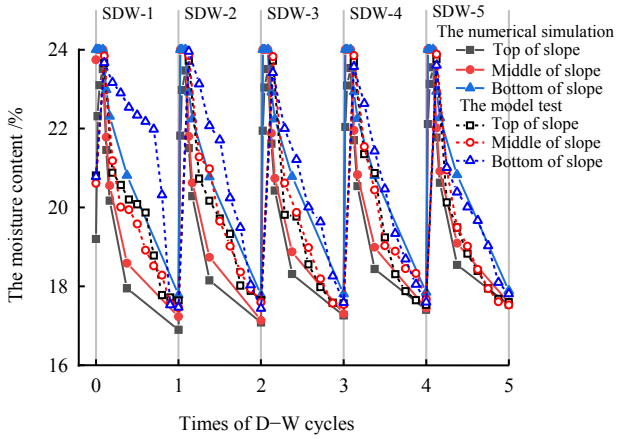


**Fig. 15 Change of slope water content under minor circulation (without cracks)**

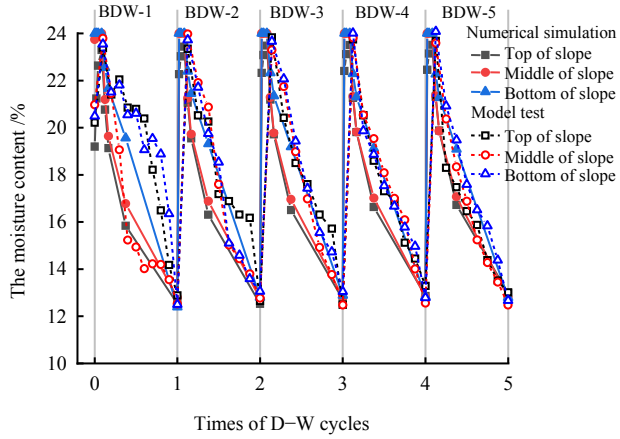


**Fig. 16 Change of slope water content under the large cycle**

In Fig. 16, the model test was conducted with a large circulation amplitude. The water content in the middle of slope decreased significantly, which reached 14.9% after drying 12 h, but the top and bottom position of water content changes slowly, mainly because the sensors installed in backfill soil is not fully compacted, where preferred main crack developed in the slope, as shown in Fig. 17. The water evaporation channel is opened rapidly, the crack expands, and the water content decreases significantly. However, with the increase of times of W−D cycles, the changes of water content in each position of slope tend to be consistent.

### 5.2 The deformation response

During the model test, the deformation of the model was observed through the transparent side. At the end of each D−W cycle, the slope contour was recorded with a marker on the transparent board (as shown in Fig. 18) and the deformation at the top, middle and bottom of the slope was measured.

**Fig. 17 Main cracks in the middle of the slope**

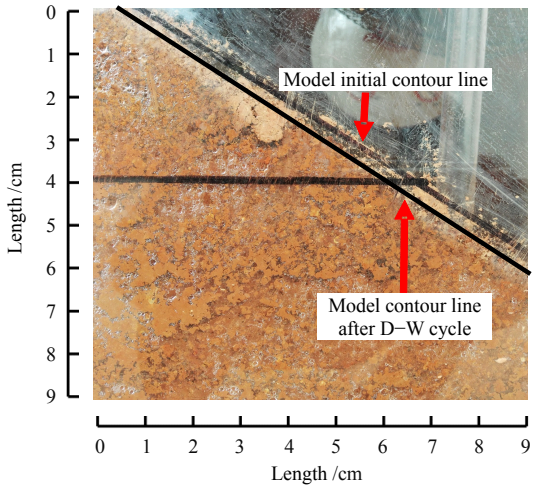


**Fig. 18 Contour line of slope**

During the entire model test, the contour line of the slope model rose after the wetting process and fell after the drying process, with a variation range of 11 mm. Meanwhile, with the increase of times of D−W cycles, the slope profile gradually moved downward, the slope top profile sank by 7.6 mm, and the middle and bottom of the slope profile sank by 6.1 mm.

The comparison of numerical simulation deformation

results is shown in Fig. 19 (Since there is a transparent plate, only the deformation of the cracked slope and the non-cracked slope under the large circulation amplitude is discussed). As can be seen from Fig. 19, the deformation behavior of slope numerical simulation and model test is the same, that is, each part of the slope rises in the wetting process and falls in the drying process. With the increase of times of D−W cycles, the difference between deformation at the top and bottom of the slope becomes larger. Compared with the results of the model test, the displacement of the numerical simulation is larger, which is mainly because the values of cohesion and internal friction angle of each soil layer are conservative in the numerical simulation. Therefore, there is a certain safety margin in the analysis of the field conditions.

The numerical simulation results show that in the slope model without considering the development of cracks, the subsidence at the top of the slope is 3.4 mm after the first cycle, which is 0.8 mm larger than that at the bottom of the slope of 2.6 mm. After the end of the fifth cycle, the slope top subsidence reached 8.0 mm, which increased by 1.5 mm compared with the slope bottom settlement of 6.5 mm. In the slope model that considering the development of cracks, after the first cycle, the subsidence at the top of the slope is 3.8 mm, which is 1.0 mm larger than that at the bottom of the slope, which is 2.8 mm. After the end of the fifth cycle, the slope top subsidence reached 8.7mm, which increased by 2.2mm compared with the slope bottom subsidence of 6.5mm.

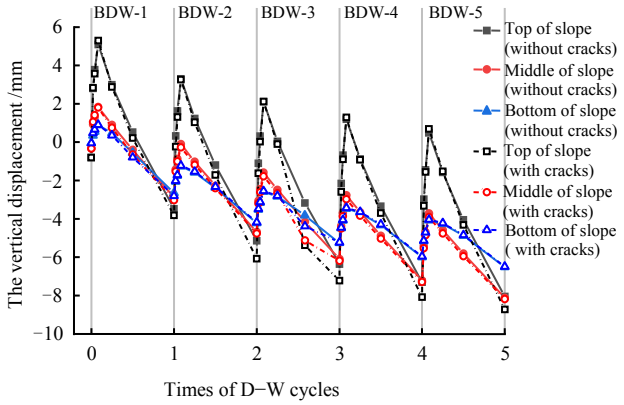


**Fig. 19 Displacement of the slope**

The difference of slope deformation with and without the influence of cracks is mainly reflected in the slope top region with the development of main cracks. During the wetting process, the deformation of the slope roof with the existence of cracks changes rapidly, but the final deformation is close to that without the existence of cracks. During the drying process, the slope with cracks deforms faster, and the final deformation is greater than that without cracks (after the end of the fifth D−W cycle, the slope top subsidence is 8.7 mm with cracks and 8.0 mm without cracks). By comparing the deformation difference between the top and the bottom of the slope under the two conditions, it can be seen that the deformation difference between the top and the bottom of the slope is 2.2 mm with the consideration of cracks, which is significantly larger than the 1.5 mm without the consideration of cracks, indicating that the development of cracks accelerates the downward trend of the top region.

## 6 Conclusion

In this paper, the relationship between the crack propagation degree and the D−W cycle is obtained by processing crack images. Considering the reduction of soil strength caused by the D−W cycle, the calculation formula of cracks depth is deduced and the influence range of cracks is determined. A numerical model is established to analyze the response characteristics of residual soil slope with cracks. After comparing with the actual model test, the conclusions are as follows:

(1) The D−W cycle can cause crack propagation in residual soil. The increase of fracture area and times of D−W cycles are in accordance with the Logistic model. With the increasing of times of D−W cycles, the cracks propagation depth gradually slows down and tends to be stable. Meanwhile, there is a quantitative relationship between the crack depths and times of D−W cycles. The crack propagation is faster under the large cycle amplitude, but the final crack propagation is consistent with that under small cyclic amplitude.

(2) The effect of D−W cycles makes the soil more and more dense, and the deformation amplitude at the top of the slope is greater than that at the bottom of the slope, and the slope has a downward trend in a whole. When the time of D−W cycles are relatively small, the response characteristics of water content at each position of residual soil slope is different: the response characteristics at the bottom of slope lags significantly behind that at the top. With the increasing of times of D−W cycles, the cracks expands, and the water content at each position of the slope tends to be consistent.

(3) The propagation behavior of cracks has the effect on the deformation of slope at each position. With the increasing of times of D−W cycles, the deformation at the bottom and middle of the slope with the crack propagation considered tends to be consistent with that without cracks, but the deformation at the top area was larger, which led to the increase of the deformation gap between the top and bottom of slope with cracks.

## References

[1] WANG Qing, TANG Da-xiong, ZHANG Qing-yun, et al. A study on the structure and composition of granite residual soil in the eastern China[J]. Journal of Changchun University of Earth Science, 1991, 21(1): 75−83.

[2] CHENG Chang-bing, XU Chang-wei. Property of the cementing material and its influence on mechanical characteristics for residual soil from granite[J]. Rock and Soil Mechanics, 1986, 7(2): 64−69.

[3] YU Jia-jing, CHEN Dong-xia, WANG Hui, et al. Analysis of the shear strength of granite residual soil and slope stability under wetting-drying cycles[J]. Journal of Xiamen University (Natural Science), 2019, 58(4): 614−620.

[4] LIU Kuan, YE Wan-jun, GAO Hai-jun, et al. Multi-scale effects of mechanical property degradation of expansive soils under drying-wetting environments[J]. Chinese Journal of Rock Mechanics and Engineering, 2020, 39(10): 2148−2159.

[5] LI H D, TANG C S, CHENG Q, et al. Tensile strength of clayey soil and the strain analysis based on image processing techniques[J]. Engineering Geology, 2019, 253: 137−148.

[6] TANG Lian-sheng, SANG Hai-tao, SONG Jing, et al. Research on soil particle joint function and brittle-elastoplastic cement damage model of unsaturated granite residual soil[J]. Rock and Soil Mechanics, 2013, 34(10): 2877−2888.

[7] MORRIS P H, GRAHAM J, WILLIAMS D J. Cracking in drying soils[J]. Canadian Geotechnical Journal, 1992, 29(2): 263−277.

[8] ALBRECHT B A, BENSON C H. Effect of desiccation on compacted natural clays[J]. Journal of Geotechnical & Geoenvironmental Engineering, 2001, 128(1): 67−75.

[9] TANG C S, SHI B, LIU C, et al. Influencing factors of geometrical structure of surface shrinkage cracks in clayey soils[J]. Engineering Geology, 2008, 101(3−4): 204−217.

[10] LOZADA C, CAICEDO B, THOREL L. Effects of cracks and desiccation on the bearing capacity of soil deposits[J]. Géotechnique Letters, 2015, 5(3): 112−117.

[11] AN N, TANG C S, XU S K, et al. Effects of soil characteristics on moisture evaporation[J]. Engineering Geology, 2018, 239: 126−135.

[12] JING N J, TANG C S, YIN L Y, et al. Applicability of microbial calcification method for sandy-slope surface erosion control[J]. Journal of Materials in Civil Engineering, 2019, 31(11): 04019250.1-04019250.11.

[13] TANG C S, SHI B, LIU C, et al. Experimental characterization of shrinkage and desiccation cracking in thin clay layer[J]. Applied Clay Science, 2011, 52(1-2): 69−77.

[14] JIAN Wen-bin, HUANG Cong-hui, LUO Yang-hua, et al. Experimental study on wetting front migration induced by rainfall infiltration in unsaturated eluvial and residual soil[J]. Rock and Soil Mechanics, 2020, 41(4): 1123−1133.

[15] WANG Jun, GONG Bi-wei, ZHANG Jia-jun, et al. Field observation and description method of cracks development on expansive rock[J]. Journal of Yangize River Scientific Research, 2010, 27(9): 78−82.

[16] LI Wei, LIU Guan-shi, YAO Ting. Improvement of methods for crack image processing and crack feature extraction of expansive soil[J]. Rock and Soil Mechanics, 2014, 35(12): 280−287.

[17] WEI Bing-xu, LIU Bin, LIU Xiong. Research on the quantitative basic index of expansive soil cracks[J]. Hydrogeology and Engineering Geology, 2015, 42(5): 90−95.

[18] LEVATTI H U, PRAT P C, LEDESMA A. Numerical and experimental study of initiation and propagation of desiccation cracks in clayey soils[J]. Computers and Geotechnics, 2018, 105:155−167.

[19] LU Zai-hua, CHEN Zheng-han, PU Yi-bin. A CT study on the crack evolution of expansive soil during drying and wetting cycles[J]. Rock and Soil Mechanics, 2002, 23(4): 417−422.

[20] ZHANG Jia-jun, GONG Bi-wei, HU Bo, et al. Study of evolution law of fissures of expansive clay under wetting and drying cycles[J]. Rock and Soil Mechanics, 2011, 32(9): 2729−2734.

[21] CHENG Q, TANG C S, ZENG H, et al. Effects of microstructure on desiccation cracking of a compacted soil[J]. Engineering Geology, 2020, 265: 105418.

[22] TANG C S, SHI B, LIU C, et al. Influencing factors of geometrical structure of surface shrinkage cracks in clayey soils[J]. Engineering Geology, 2008, 101(3-4): 204−217.

[23] HU Dong-xu, LI Xian, ZHOU Chao-yun, et al. Quantitative analysis of swelling and shrinkage cracks in expansive soil[J]. Rock and Soil Mechanics, 2018, 39(Suppl.1): 327−333.

[24] WANG Jian-li, LUO Yi, LÜ Shao-quan, et al. Experimental study on cracks evolution laws of non-saturated weak expansive soil under natural evaporation[J]. Geotechnical Investigation and Surveying, 2019, 47(6): 16−22.

[25] WEI Bing-xu, HUANG Zhen, GAO Bing, et al. Crack evolution rules of expansive soil and the effect on the shear strength under the action of dry-wet circulation[J]. Highway Engineering, 2015, 40(4): 131−134, 144.

[26] CHEN Kai-sheng. Evolution of cracks in red clay under wetting-drying cycles and its influence on shear strength[J]. Hydrogeology and Engineering Geology, 2018, 45(1): 95−101.

[27] TANG C S, CHENG Q, LENG T, et al. Effects of wetting-drying cycles and desiccation cracks on mechanical behavior of an unsaturated soil[J]. Catena, 2020, 194:104721.

[28] LU N, KIM T H, STURE S, et al. Tensile strength of unsaturated sand[J]. Journal of Engineering Mechanics, 2009, 135(12): 1410−1419.

[29] SHI B X, CHEN S S, WANG G L. Computation module of expansive soil crack depth considering dry-wet cycles[C]//Geo-Hubei 2014 International Conference on Sustainable Civil Infrastructure. Yichang: [s. n.], 2014.

[30] SHI B X, CHEN S S. Expansive soil crack depth under cumulative damage[J]. The Scientific World Journal, 2014, 12: 1−9.

[31] THI D V, AMADE P, SAHAR H, et al. Numerical modelling of desiccation cracking of clayey soil using a cohesive fracture method[J]. Computers and Geotechnics, 2017, 85: 15−27.

[32] HUANG Qiang. Yearbook of Xiamen special economic zone: rainfall, evaporation and humidity in the island[M]. Beijing: China Statistics Press, 2020.

[33] TANG Lian-sheng, SANG Hai-tao, HOU Tao, et al. Experimental study on tensile strength of granite residual soil[J]. Acta Scientiarum Naturalium Universitatis Sunyatseni, 2014, 53(6): 104−111.

[34] CHEN Dong-xia. Study on soil water characteristics and strength characteristics of unsaturated residual soil in Xiamen[D]. Hangzhou: Zhejiang University, 2014.

[35] LI Pei-yong, YANG Qing, LUAN Mao-tian, et al. Research on influential factors of crack propagation depth of unsaturated expansive soils[J]. Chinese Journal of Rock Mechanics and Engineering, 2008, 27(Suppl. 1): 2967−2972.

[36] YIN Zong-ze, XU Bin. Slope stability of expansive soil under fissure influence[J]. Chinese Journal of Geotechnical Engineering, 2011, 33(3): 454−459.

[37] LIU Hong-tai, ZHANG Ai-jun, DUAN Tao, et al. The influence of alternate dry-wet on the strength and permeability of remolded loess[J]. Hydro-Science and Engineering, 2010, 12(4): 38−42.

[38] ZHANG Jia-jun. Study of the fissures, volume change and permeability of expansive soil under wetting and drying cycles[D]. Guangzhou: South China University of Technology, 2010.

[39] YUAN Jun-ping, LIN Yan-ling, DING Peng, et al. Influence of anisotropy induced by fissures on rainfall infiltration of slopes[J]. Chinese Journal of Geotechnical Engineering, 2016, 38(1): 76−82.